IEEE Access
Multidisciplinary | Rapid Review | Open Access Journal

Received March 10, 2022, accepted March 22, 2022, date of publication March 30, 2022, date of current version April 6, 2022.

Digital Object Identifier 10.1109/ACCESS.2022.3163306

Nonlinear Robust Control of Unknown Robot Manipulator Systems With Actuators and Disturbances Using System Identification and Integral Sliding Mode Disturbance Observer

DONGKYOUNG CHWA[1] AND HEEJUN KWON[2]
[1]Department of Electrical and Computer Engineering, Ajou University, Suwon-si 443-749, South Korea
[2]FASTECH, Pyeongcheon-ro, Bucheon-si, Gyeonggi-do 14502, South Korea

Corresponding author: Dongkyoung Chwa (dkchwa@ajou.ac.kr)

This work was supported by the National Research Foundation of Korea (NRF) Grant funded by the Korea Government [Ministry of Science and ICT (MSIT)] under Grant 2020R1A2C101226111.

ABSTRACT In this study, nonlinear robust control of robot manipulator systems with completely unknown manipulator dynamics using a system identification and integral sliding mode disturbance observer (SI-ISMDOB)-based sliding mode control (SMC) method is proposed. Because the unknown robot manipulator system—owing to the actuator dynamics, unknown manipulator parameters, frictional forces, and unknown load torques—cannot be controlled using the existing model-based methods, they need to be identified; subsequently, the identified manipulator system should be controlled in a robust manner. To this end, the manipulator-actuator dynamics at the motor shaft are first proposed by considering the unknown robot manipulator dynamics as torque disturbances and are subsequently identified using the system identification. An SI-ISMDOB-based SMC method is then developed using the identified manipulator-actuator dynamics and torque-disturbance estimates from the ISMDOB. The simulation and experimental results on an actual planar manipulator system are presented to verify the improved performance of the proposed method over the SMC method and SMDOB-based SMC method via a performance indicator.

INDEX TERMS Integral sliding mode disturbance observer-based sliding mode control, manipulator-actuator dynamics, nonlinear robust control, system identification, unknown robot manipulator system.

LIST OF SYMBOLS AND ABBREVIATIONS

v	armature voltage input
v_d	disturbance compensation voltage input
v_c	SMC voltage input
I	armature current
τ_m	torque developed by the motor
τ_d	load torque at the motor shaft
τ	control torque on the joint of the manipulator
θ_m	motor shaft position
θ	actual joint position measured by the encoder
θ_r	reference joint position
J_m	moment of inertia of the motor shaft
J	moment of inertia of the actuator
B_m	viscous friction coefficient of the motor shaft
B	viscous friction coefficient of the actuator
K_t	torque constant
K_e	counter electromotive force constant
L, R	inductance, resistance
n, η	gear ratio, efficiency of the gearbox
R	resistance
$\hat{\theta}_s$	estimate of $\theta_s(:=\dot{\theta})$
$\hat{\Omega}$	estimate of the disturbance Ω
e_o	estimation error defined as $\theta_s - \hat{\theta}_s$
s	sliding surface
s_{oI}	integral sliding surface
SI	system identification
SMC	sliding mode control
TSMC	terminal sliding mode control
ISMC	integral sliding mode control
DOB	disturbance observer
SMDOB	sliding mode disturbance observer
ISMDOB	integral sliding mode disturbance observer

The associate editor coordinating the review of this manuscript and approving it for publication was Jinquan Xu.

I. INTRODUCTION

Robot manipulator systems, which are widely used in industries, must have significantly high precision [1]. Robust control strategies are needed to ensure that the effects of various work environments, such as the unknown varying weights of the loads attached to the end effector of a manipulator, do not degrade their tracking performance. Therefore, adaptive and robust control strategies have been proposed to compensate for the uncertainties and maintain the tracking performance. In particular, sliding mode control (SMC) methods are proposed by introducing the sliding surfaces in [2]–[6] and adaptive SMC methods that combine the adaptive algorithms and SMC methods are studied in [7]–[10]. In addition, terminal SMC (TSMC) methods in [11]–[14] can guarantee the finite time convergence of the states unlike the SMC, and super twisting SMC method [15] can reduce chattering owing to the switching function while maintaining the robustness against varying parameter. Since the disturbance observers (DOBs) can achieve robust manipulator control, various DOBs have also been designed in [16]–[19] to estimate and compensate for system disturbances. Various studies on the compensation of the uncertainties in the manipulator dynamics and the disturbances arising from the unknown load torque have also been proposed by using intelligent control techniques to estimate the disturbances and uncertainties. In particular, neural network based methods are proposed in [20]–[22] and adaptive fuzzy control methods are studied in [23]–[25]. The combination of neural network and adaptive fuzzy control methods are also designed in [26], [27] and swarm optimization based method is proposed in [28]. In order to obtain the robustness in the intelligent control methods, neural network-based SMC methods are developed in [29]–[31]. Reinforcement learning control method is also designed in [32]. Although the equations representing the dynamics of robot manipulator systems are used in the aforementioned existing methods for designing manipulator controllers, the presence of actuator dynamics, unknown manipulator parameters, frictional forces, and unknown load torque results in the significant degradation of the control performance.

The modeling of the *unknown manipulator system* (i.e., robot manipulator system with unknown dynamics) is difficult in practice owing to the following reasons. The dynamics of the actuators in the robot, which are required for the implementation of a robot manipulator in an actual environment, have considerable influence on the manipulator performance and should be included in the manipulator dynamics. In addition, because precise values of the inertial parameters of the links constituting the manipulator cannot be readily obtained, the resulting overall robot manipulator dynamics are complicated and difficult to obtain. Several studies ([20]–[29]) have considered a few of these issues and are based on model-based control methods in which nominal manipulator dynamics are still required. Although the adaptive decentralized manipulator control methods proposed in [33], [34] do not require the manipulator dynamics for control, and the resulting residual dynamics are considered as uncertainties, the effects of the uncertainties are significant in this case; thus, the uncertainties cannot be sufficiently compensated by SMC and DOBs, as will be verified in the experimental results of this study.

The present work is motivated by the fact that: i) the performance degraded by the unknown actuator dynamics, unknown manipulator parameters, frictional forces, and unknown load torques should be recovered, and ii) the unknown manipulator system should be modeled and controlled in a robust manner.

The objectives of this study are i) development and identification of manipulator-actuator dynamics for an unknown robot manipulator system, considering the actuator dynamics, unknown manipulator parameters, frictional forces, and unknown load torques; ii) enhancement of the control performance of the unknown robot manipulator system, which is degraded by the unknown actuator dynamics, unknown manipulator parameters, frictional forces, and unknown load torques; and iii) development of a nonlinear robust control method based on system identification [35] and a robust disturbance observer for the unknown manipulator.

This paper presents a system identification and integral sliding mode disturbance observer (SI-ISMDOB)-based SMC method for the unknown manipulator system. The overall structure of the proposed SI-ISMDOB-based robust control method for the unknown robot manipulator is shown in Fig. 1.

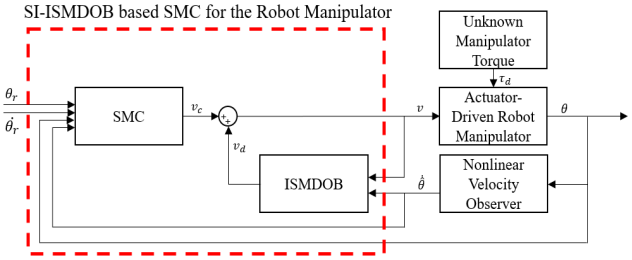

FIGURE 1. Structure of the proposed SI-ISMDOB-based nonlinear robust control system for the unknown robot manipulator.

Unlike the existing model-based control studies based on the manipulator dynamics, the proposed method is based on the manipulator-actuator dynamics that are obtained by considering the manipulator dynamics as torque disturbances and combining the manipulator and actuator dynamics at the motor shaft. Considering the unspecified parameters of actuator systems, system identification was performed to identify the manipulator-actuator dynamics. To compensate for the torque disturbances, an integral sliding mode DOB (ISMDOB) was designed based on the identified manipulator-actuator dynamics. An SI-ISMDOB-based SMC law was then designed using the torque disturbance estimates obtained from the ISMDOB. Owing to the difficulty of reliably obtaining the joint velocities by differentiating the joint positions

measured from the encoders, a velocity observer was additionally used in the experiments.

The contributions of the proposed method are as follows.

First, manipulator–actuator dynamics, which combine manipulator and actuator dynamics, are proposed by considering the motion of the robot manipulator as a disturbance. Although existing control methods for robot manipulators ([1]–[19]) do not include the actuator dynamics in the robot manipulator dynamics, they must be included during the controller design owing to their significant impact on the performance of the manipulator system. The actuator dynamics have been considered in the manipulator control in [20]–[29], which, however, require knowledge of the manipulator dynamics, actuator dynamics, frictional forces, and unknown parameters constituting the manipulator, which cannot be readily obtained. Accordingly, these issues cannot be resolved by using the existing manipulator control methods. Owing to these problems, the manipulator-actuator dynamics have been identified via system identification method in [35] by considering the torques generated from the manipulator links as disturbances such that the manipulator control can be achieved without the information on the manipulator dynamics.

Second, an ISMDOB is proposed to estimate the torque disturbances in the manipulator-actuator dynamics such that the estimates are used in the control law for the identified manipulator-actuator dynamics. Because the ISMDOB employs a robust disturbance compensation term, the estimation performance can be maintained irrespective of the time-varying characteristics of the disturbances. In particular, an ISMDOB uses the integral sliding mode [36], [37] such that the sliding surface can be reached from the start and the uncertainties can be compensated at all times, unlike DOBs ([16]–[18]) and sliding mode DOB (SMDOB) [38].

Third, a nonlinear robust control law using SI-ISMDOB-based SMC is proposed for the manipulator using the disturbance estimates obtained by the proposed ISMDOB. While offline identification is used to achieve satisfactory transient tracking control performance, the online adaptation to the uncertainties owing to both the identification error and disturbances was achieved by the proposed SI-ISMDOB-based SMC method. As the disturbances resulting from the manipulator motion increase in magnitude, the performance of the SMC with the adjustment of the switching control gain decreases. In contrast, by constantly attaining the robustness against the identification errors and disturbances using the disturbance estimates in the proposed control law, the control performance of the proposed SI-ISMDOB-based SMC law can be greatly improved compared with both the SMC law and the SMDOB-based SMC law that uses the disturbance estimates from the SMDOB [38].

Finally, the experimental results obtained using an actual robot manipulator are presented to validate the proposed modeling and system identification of the manipulator-actuator dynamics and the proposed SI-ISMDOB-based SMC method. Because the manipulator-actuator model has a voltage input instead of torque input owing to the inclusion of the actuator dynamics, the proposed method can be readily implemented. When an additional load is attached to the end effector of the manipulator, the proposed method can achieve considerably improved performance over the SMC method and SMDOB-based SMC method, validating the robustness of the proposed method.

II. MODELING OF MANIPULATOR-ACTUATOR DYNAMICS

In this section, the proposed modeling of manipulator-actuator dynamics under the condition that the actuator system driving the manipulator is a DC motor is presented. The manipulator and actuator dynamics can be expressed as [25], [32]

$$J_m\ddot{\theta}_m + B_m\dot{\theta}_m + \tau_d = \tau_m, \quad \tau_m = K_t I, \tag{1}$$

$$L\dot{I} + RI = v - K_e\dot{\theta}_m. \tag{2}$$

The effect of the inductance L in (2) is relatively small compared with the mechanical motion in (1). In addition, the dynamic model needs to be modified when a gearbox is attached to the motor driving the manipulator system, that is, τ_d and θ_m are respectively related to τ and θ as

$$\tau = \eta n \tau_d, \quad \dot{\theta}_m = n\dot{\theta}. \tag{3}$$

Therefore, (1), (2), and (3) can be combined as

$$J\ddot{\theta} + B\dot{\theta} + \tau = \eta n K_t I, \tag{4}$$

$$RI = v - nK_e\dot{\theta}, \tag{5}$$

where J and B are the moment of inertia and coefficient of viscous friction of the actuator dynamics, respectively. Combination of (4) and (5) yields

$$\ddot{\theta} + \frac{1}{J}\left(B + \frac{\eta n^2 K_t K_e}{R}\right)\dot{\theta} + \frac{\tau}{J} = \frac{\eta n K_t}{JR} v, \tag{6}$$

where τ is considered as the torque disturbance in the combined manipulator and actuator dynamics.

Remark 1: The time-varying characteristics of τ in (6) can be observed as follows: Assuming a uniform mass distribution for each link of the manipulator, the dynamic equations for a two-link manipulator are given by [25], [32]

$$\boldsymbol{M}(\theta)\ddot{\theta} + \boldsymbol{C}\left(\theta, \dot{\theta}\right) + \boldsymbol{G}(\theta) = \tau, \tag{7}$$

where $\boldsymbol{M}(\theta)$, M_{11}, $\boldsymbol{C}\left(\theta, \dot{\theta}\right)$, and $\boldsymbol{G}(\theta)$, as shown at the bottom of the next page. Here, m_i and l_i are the mass and length of i-th link for $i = 1, 2$, respectively, and g is the gravitational acceleration. It should be noted that many robot manipulator systems with n joints can be modeled in the form of (7), because each actuator at each joint can control each link attached at the joint by considering the manipulator dynamics as torque disturbances. Therefore, the proposed method can also be used in general manipulator systems.

By defining $x_1 = \theta$ and $x_2 = \dot{\theta}$, (6) can be expressed as the manipulator-actuator dynamics given by

$$\dot{x}_1 = x_2, \dot{x}_2 = \frac{\eta n K_t}{JR} v - \frac{1}{J}\left(B + \frac{\eta n^2 K_t K_e}{R}\right) x_2 - \frac{\tau}{J}. \tag{8}$$

The voltage input can then be designed as

$$v := v_d + v_c \tag{9}$$

by combining the SI-ISMDOB-based disturbance compensation input v_d and SMC input v_c which will be designed later in (18) and (31), respectively. The torque disturbance τ in (8) mainly arises from the manipulator dynamics in (7), but it can include all the modeling errors in the manipulator-actuator dynamics, unknown time-varying parameters, and frictional forces.

Remark 2: The torque disturbance τ and load torque at the motor shaft τ_d are related by (3). Because the exact value of τ is not known, τ in (8) is estimated using an ISMDOB in Section III.A.

III. NONLINEAR ROBUST CONTROL BASED ON ISMDOB FOR AN UNKNOWN ROBOT MANIPULATOR

Section III.A presents the design of ISMDOB on the basis of the robot manipulator-actuator dynamics in (8) to estimate the torque disturbances. An SI-ISMDOB-based SMC law is then designed in Section III.B using the disturbance estimates to compensate for the torque disturbances. The manipulator-actuator system parameters in (8) required for the controller design are obtained by system identification in Section III.C.

A. ISMDOB BASED ON MANIPULATOR-ACTUATOR DYNAMICS

An ISMDOB is used to estimate the torque disturbance τ in (7). Thus, the manipulator-actuator dynamics in (8) can be rewritten as

$$\dot{\theta}_s = F + \Omega, \tag{10}$$

where $\theta_s = \dot{\theta}$, $F = \frac{\eta n K_t}{JR}(v_c + v_d) - \frac{1}{J}\left(B + \frac{\eta n^2 K_t K_e}{R}\right)\theta_s$ is a known function, and $\Omega := -\frac{\tau}{J}$ is a disturbance that needs to be estimated and compensated. Considering that τ originates from the manipulator system in the manipulator-actuator dynamics, the following assumption is made:

Assumption 1: The torque disturbance τ and its time derivative are bounded.

The validity of Assumption 1 is obvious from the fact that the voltage input is physically bounded; thus, the torque, that is, the output of the actuator, and its time derivative are also physically bounded by this practical power supply limitation.

To estimate the disturbance Ω in (10), the disturbance observation model is defined as [38]

$$\dot{\hat{\theta}}_s = F + \hat{\Omega}, \tag{11}$$

where $\hat{\theta}_s$ and $\hat{\Omega} := -\hat{\tau}/J$ are the estimates of θ_s and Ω, respectively. The integral sliding surface is then defined with respect to the estimation error $e_o := \theta_s - \hat{\theta}_s$ as [36]

$$s_{oI} = e_o + e_{oI}, \tag{12}$$

where

$$\dot{e}_{oI} = \gamma tanh\{(a+bt)\, e_o\}, \tag{13}$$

with the initial condition $e_{oI}(0) = -e_o(0)$ such that $s_{oI}(0) = 0$ holds. It should be noted that because $e_o(0)$ and $e_o(t)$ are available owing to the known values of θ_s and $\hat{\theta}_s$, e_{oI} can be obtained by integrating (13) such that $s_{oI}(0) = 0$ and $s_{oI}(t)$ can be maintained at zero, the validity of which along with the derivation of (13) is shown in the proof of Theorem 1. The ISMDOB can then be designed as

$$\hat{\Omega} = k s_{oI} - \bar{v} + \gamma tanh\{(a+bt)\, e_o\}, \tag{14}$$

$$\dot{\bar{v}} = u, \tag{15}$$

$$\begin{aligned} u = {} & \gamma sech^2\{(a+bt)\, s_{oI} \cdot < (a+bt)\,[\hat{\Omega} - \gamma \\ & tanh\{(a+bt)\, e_o\}] - b s_{oI} > -\gamma^2 (a+bt) \\ & \cdot sech^2\{(a+bt)\, s_{oI}\}\, sgn(s_o) - \bar{k}\, sgn(s_o) - s_{oI}, \end{aligned} \tag{16}$$

and the sliding surface s_o is given by

$$s_o = \bar{v} + \gamma tanh(a+bt)\, s_{oI} \tag{17}$$

for positive constants a, b, $\bar{k}$, and γ satisfying $\gamma > \Omega$, and the initial condition $v(0) = -\gamma tanh\{a s_o(0)\}$, such that $s_o(0) = 0$. The performance of the proposed ISMDOB is analyzed, and the disturbance compensation input v_d is designed in Theorem 1.

Theorem 1 (ISMDOB for the Estimation of Torque Disturbance): Under Assumption 1, the ISMDOB in (11)–(17) guarantees the asymptotic convergence of s_{oI}, e_o, and $\dot{e}_o$ to zero such that $\hat{\Omega}$ asymptotically converges to Ω. The control input v_d for the disturbance compensation can then be designed as

$$v_d = -\frac{JR}{\eta n K_t}\hat{\Omega}, \tag{18}$$

which leads to $v_d = \frac{R}{\eta n K_t}\hat{\tau}$ from (11).

$$\boldsymbol{M}(\theta) = \begin{bmatrix} M_{11} & m_2 l_2^2/3 + m_2 l_1 l_2 \cos\theta_2/2 \\ m_2 l_2^2/3 + m_2 l_1 l_2 \cos\theta_2/2 & m_2 l_2^2/3 \end{bmatrix},$$

$$M_{11} = (m_1 l_1^2 + m_2 l_2^2)/3 + m_2 l_1^2 + m_2 l_1 l_2 \cos\theta_2,$$

$$\boldsymbol{C}(\theta, \dot{\theta}) = \begin{bmatrix} -m_2 l_1 l_2 \dot{\theta}_2^2 \sin\theta_2/2 - m_2 l_1 l_2 \dot{\theta}_1 \dot{\theta}_2 \sin\theta_2 \\ m_2 l_1 l_2 \dot{\theta}_1^2 \sin\theta_2/2 \end{bmatrix}$$

$$\boldsymbol{G}(\theta) = \begin{bmatrix} (m_1/2 + m_2) g l_1 \sin\theta_1 + m_2 g l_2 \sin(\theta_1 + \theta_2)/2 \\ m_2 g l_2 \sin(\theta_1 + \theta_2)/2 \end{bmatrix}.$$

Proof: The time derivative of the sliding surface s_{oI} in (12) can be combined with (10), (11), and (13) to obtain

$$\dot{s}_{oI} = \Omega - \hat{\Omega} + \gamma tanh\{(a+bt)\, e_o\}, \tag{19}$$

which, in turn, can be expressed using (14) and (17) as

$$\begin{aligned} \dot{s}_{oI} &= \Omega - k s_{oI} + \bar{v} \\ &= \Omega - k s_{oI} + s_o - \gamma tanh\{(a+bt)\, s_{oI}\}. \end{aligned} \tag{20}$$

The time derivative of the Lyapunov function $V_1 = s_{oI}^2/2$ can then be obtained using (20) as:

$$\begin{aligned} \dot{V}_1 &= s_{oI}\dot{s}_{oI} \\ &= s_{oI}[\Omega - k s_{oI} + s_o - \gamma tanh\{(a+bt)\, s_{oI}\}] \\ &\le -k s_{oI}^2 + s_{oI} s_o - \gamma\, |s_{oI}| \cdot [tanh\{(a+bt)\, |s_{oI}|\} - \alpha], \end{aligned} \tag{21}$$

where $0 \le \alpha := \Omega/\gamma < 1$.

The time derivative of s_o in (17) can be expressed as

$$\begin{aligned} \dot{s}_o &= u + \gamma sech^2\{(a+bt)\, s_{oI}\} < (a+bt) \\ &\quad \times [\Omega - \hat{\Omega} + \gamma tanh\{(a+bt)\, e_o\}] + b s_{oI} > . \end{aligned} \tag{22}$$

Substitution of (16) into (22) gives

$$\begin{aligned} \dot{s}_o &= \gamma sech^2\left\{(a+bt) s_{oI}\right\}(a+bt)\Omega - \gamma^2 (a+bt) \\ &\quad \cdot sech^2\{(a+bt)\, s_{oI}\} sgn\,(s_o) - \bar{k} sgn\,(s_o) - s_{oI}. \end{aligned} \tag{23}$$

The time derivative of another Lyapunov function $V_2 = s_o^2/2$ can then be obtained as

$$\begin{aligned} \dot{V}_2 &= s_o \dot{s}_o \\ &= \gamma s_o sech^2(a+bt) s_{oI} \cdot (a+bt)\Omega - \gamma^2 (a+bt) \\ &\quad \cdot sech^2\{(a+bt)\, s_{oI}\}\, |s_o| - \bar{k}\, |s_o| - s_{oI} s_o \\ &\le -\bar{k}\, |s_o| - s_{oI} s_o. \end{aligned} \tag{24}$$

The time derivative of the total Lyapunov function $V_o := V_1 + V_2$ can be obtained from (21) and (24) as

$$\begin{aligned} \dot{V}_o \le & -k s_{oI}^2 - \bar{k}\, |s_o| \\ & - \gamma\, |s_{oI}|\, [tanh\{a+bt)|s_{ol}|\}] - \alpha]. \end{aligned} \tag{25}$$

In the case where $|s_{oI}| \ge \frac{1}{2(a+bt)} \ln\left(\frac{1+\alpha}{1-\alpha}\right)$, the following relationship is satisfied:

$$tanh\{(a+bt)\, |s_{oI}|\} \ge \alpha, \tag{26}$$

in which case the inequality in (25) satisfies

$$\dot{V}_o \le -k s_{oI}^2 - \bar{k}\, |s_o|. \tag{27}$$

Accordingly, s_{oI} and s_o are ultimately bounded, and their ultimate bounds decrease to zero owing to the fact that the relationship in (26) holds with increasing time. From (27), $s_{oI}, s_o \in L_\infty$, and $s_{oI} \in L_2$. Moreover, $\dot{s}_{oI} \in L_\infty$ holds from (19) and Assumption 1. Therefore, s_{oI} asymptotically converges to zero as per Barbalat's lemma [39]. The boundedness of $\ddot{s}_{oI}$ can also be derived to show that $\dot{s}_{oI}$ and thus e_o asymptotically converge to zero, which implies the convergence of $\hat{\Omega}$ to Ω. Therefore, the additional input v_d using $\hat{\Omega}$ generated from the ISMDOB can be designed based on (11) to satisfy

$$\frac{\eta n K_t}{JR} v_d + \hat{\Omega} = 0, \tag{28}$$

which results in (18). ■

B. SI-ISMDOB-BASED SMC FOR ROBUST ASYMPTOTIC TRACKING CONTROL

The tracking error variables are defined as

$$e_1 = \theta_r - x_1, \quad e_2 (:= \dot{e}_1) = \dot{\theta}_r - x_2. \tag{29}$$

In terms of the tracking errors in (29), the sliding surface is designed as [36]

$$s = k_1 e_1 + e_2. \tag{30}$$

The SI-ISMDOB-based SMC input v is then designed by respectively choosing v_d as per (18) and v_c as

$$\begin{aligned} v_c = \frac{JR}{\eta n K_t} \Bigg\{ & k_2 s + k_1 e_2 + \ddot{\theta}_r + \frac{1}{J}\left(B + \frac{\eta n^2 K_t K_e}{R}\right) x_2 \\ & + \frac{K_m tanh\{(a+bt)\, s\}}{J} \Bigg\}, \end{aligned} \tag{31}$$

where k_1, k_2, and K_m are positive constants.

Remark 3: It is well known that a signum function, which is used in the sliding mode control methods, results in the chattering phenomenon, which should be inhibited by using functions, such as a saturation function and a tangent hyperbolic function. In (31), $tanh\,(s)$ is used instead of the signum function $sgn\,(s)$ to reduce the chattering phenomenon.

The stability and performance of the overall manipulator control system using the proposed method are described in Theorem 2.

Theorem 2 (SI-ISMDOB-Based SMC): The SI-ISMDOB-based SMC law v using v_d in (18) and v_c in (31) can guarantee an asymptotic tracking control performance in the sense that s converges to zero in a finite time and e_1 asymptotically converges to zero.

Proof: The Lyapunov function $V = s^2/2$ can be differentiated with respect to time to obtain

$$\dot{V} = s\left\{k_1 e_2 + \ddot{\theta}_r - \frac{\eta n K_t}{JR} v + \frac{1}{J}\left(B + \frac{\eta n^2 K_t K_e}{R}\right) x_2 + \frac{\tau}{J}\right\}. \tag{32}$$

Substitution of (31) and (18) into (32) gives

$$\begin{aligned} \dot{V} &= -k_2 s^2 - \frac{K_m tanh\,\{(a+bt)\, s\}\, s}{J} + \frac{\tilde{\tau}}{J} s \\ &\le -k_2 s^2 - \frac{|s|}{J} \cdot [K_m tanh\,\{(a+bt)\, |s|\} - |\tilde{\tau}|] \end{aligned} \tag{33}$$

where $\tilde{\tau} := \tau - \hat{\tau}$, guaranteeing the ultimate boundedness of s. It should be noted that the ultimate bound of s is dependent on $\tilde{\tau}$, which asymptotically converges to zero as per Theorem 1. Because $|\tilde{\tau}|$ becomes less than $K_m tanh\,\{(a+bt)\, |s|\}$ in a finite time, $\dot{V} \le -\epsilon\, |s|$ holds from (33) for some $\epsilon > 0$ after a finite time, implying the finite-time stability of $s = 0$ [40].

Accordingly, e_1 asymptotically converges to zero according to (30). Because the estimation error $\tilde{\tau}$ arising from the use of ISMDOB is analyzed in $\dot{V}$ in the form of (33), the effect of the ISMDOB on the overall robot manipulator control system is considered in the stability analysis. ■

Remark 4: Although the effect of τ on the tracking performance can be suppressed by the last term in (31), the experimental results obtained using an actual robot manipulator, as presented in Section IV, demonstrate that the tracking performance of the SMC law degrades depending on the characteristics of τ, unlike the proposed SI-ISMDOB-based SMC.

C. SYSTEM IDENTIFICATION OF MANIPULATOR-ACTUATOR DYNAMICS

To design the proposed SI-ISMDOB-based SMC, the manipulator-actuator dynamics in (8) (i.e., the term F in (10)) should be known. Accordingly, the system identification toolbox provided by MATLAB was used to identify the manipulator-actuator dynamics of the system containing DC motors equipped with gearboxes. In the system identification, the transfer functions were obtained by using the DC motor voltages as inputs and their joint velocities as outputs. The structure of the identified manipulator-actuator dynamics was obtained based on the Hammerstein–Wiener model [41]–[43] using the system identification toolbox, as shown in Fig. 2.

When a voltage input v with a value of $3.5\sin(2.3t) + 2.5\cos(1.3t)$ was applied to the two DC motors, the identified models were obtained with respect to the first and second joint velocities (i.e., $\dot{\theta}_1$ and $\dot{\theta}_2$) as

$$\frac{\dot{\theta}_1(s)}{v(s)} = \frac{80.5610}{s+44.7388}, \frac{\dot{\theta}_2(s)}{v(s)} = \frac{96.9472}{s+54.8874} \tag{34}$$

with accuracies of 98.15% and 97.23%, respectively. On the other hand, the model of the manipulator-actuator dynamics in (8) can be expressed as

$$\frac{\dot{\theta}(s)}{v(s)} = \frac{\frac{\eta n K_t}{JR}}{s + \frac{1}{J}\left(B + \frac{\eta n^2 K_t K_e}{R}\right)}. \tag{35}$$

Here, K_t, K_e, and R are determined by the motor specifications, and η and n are known values, all of which are listed in Table 1 and can be substituted into (35). The values of J and B can be calculated by comparing (34) and (35) and are listed in Table 1.

TABLE 1. DC motor parameters in (8).

Motor specification parameters	System identification parameters
$K_t = 6.92\cdot10^{-3}(Nm/V)$ $K_e = 6.92\cdot10^{-3}(V/(rad/s))$ $R = 1.94\ (\Omega), n = 70, \eta = 0.8$	$J_1 = 2.6237\cdot10^{-3}(kg\cdot m^2)$ $J_2 = 2.3043\cdot10^{-3}(kg\cdot m^2)$ $B_1 = 0.0146\ (Nm\cdot s)$ $B_2 = 0.0140\ (Nm\cdot s)$

The angular velocity $\dot{\theta}$ (i.e., x_2) in (8) is not directly measurable by the encoders because taking time differentiation of the measured joint positions to obtain the joint velocities amplifies the sensor noise. The velocity estimates from the velocity observer [44] given by

$$\dot{\hat{\theta}} = p + K_0\tilde{\theta}, \dot{p} = K_1 sgn\tilde{\theta} + K_2\tilde{\theta} \tag{36}$$

are used in the experiments for positive constants K_0, K_1, and K_2.

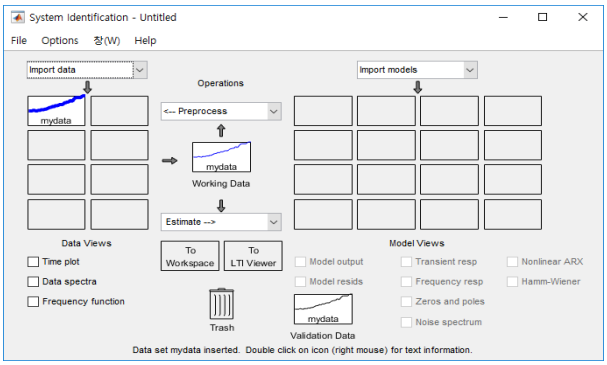

(a) Importing data and choice of nonlinear models.

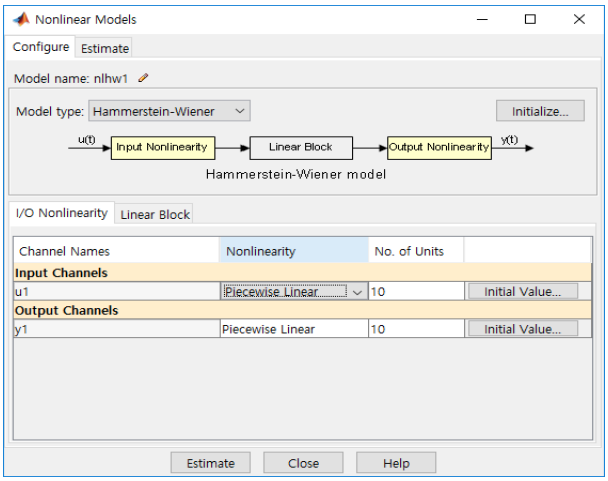

(b) Setting of Hammerstein-Wiener model.

FIGURE 2. Hammerstein-Wiener model for the identification of manipulator-actuator dynamics using system-identification toolbox.

IV. SIMULATION AND EXPERIMENTAL RESULTS

The simulation and experimental results are presented to validate the modeling of the manipulator-actuator dynamics, identification method, and SI-ISMDOB-based SMC method presented in Sections II and III. To verify the performance of the proposed method, the performances of SMC, SMDOB-based SMC [38], and the proposed SI-ISMDOB-based SMC methods are compared in this section. As the existing methods cannot be used for the unknown manipulator system and the proposed method which is based on the manipulator-actuator dynamics is critical for the development of a control method for the unknown manipulator system, the type of control method used and further development of the various ISMOs is not within the scope of this study.

TABLE 2. Manipulator system parameters in (7).

m_1	m_2	g	l_1	l_2
165.7 (g)	103.1 (g)	9.81 (m/s^2)	10.8 (cm)	15.4 (cm)

TABLE 3. Controller design parameters in (31).

K_{m1}	K_{m2}	k_1	k_2
0.7	0.4	4	4

TABLE 4. DOB design parameters in (12)–(17) and (37)–(38).

$\bar{k}$		γ		k		a		b	
SM	ISM	SM	ISM	SM	ISM	SM	ISM	SM	ISM
10	10	500	350	100	100	30	0.05	n/a	0.001

A. SIMULATION RESULTS

Simulations were performed using the MATLAB/Simulink software. The nonlinear dynamics of the robot manipulator in (7) were used in the simulations. The DC motor variables used in the simulations are listed in Table 1, and the parameters of the manipulator, controller, and DOB are summarized in Tables 2–4, respectively. The design parameters of the controller and DOBs listed in Tables 3 and 4 were chosen by trial and error by observing the control and estimation performance, as in the case of nonlinear control methods. It should be noted that SI-ISMDOB-based SMC method combines SMC with ISMDOB. Therefore, to compare the performance of the SMC method, SMDOB-based SMC method, and SI-ISMDOB-based SMC method, the design parameters of the SMC law are set to be same in all these methods for a fair comparison. However, the structures of SMDOB and ISMDOB are different from each other; thus, their design parameters cannot be the same.

To verify the tracking control performance of the proposed method, a reference sinusoidal function was applied to the first joint θ_1 for 15 s and to the second joint θ_2 for 25 s. In addition, each scenario was simulated with and without the DOBs, and their performances were compared, as shown in Fig. 3, to verify the disturbance compensation performance. The robust control using $\hat{\Omega}$ from the ISMDOB in (18) is also compared with an SMDOB [38], which is given by

$$\hat{\Omega} = ks_o - v, \quad s_o = v + \gamma tanh\,(ae_o)\,, \ \dot{v} = u, \tag{37}$$

$$u = \gamma sech^2\,(ae_o)\,a\hat{\Omega} + \gamma^2 asech^2\,(ae_o)\,sgn\,(s_o) - \bar{k}sgn\,(s_o) - s_{oI}\,. \tag{38}$$

In the case of SMC without using any DOB, noticeably large tracking errors were observed, irrespective of the form of the references, as shown in Figs. 3(a), 3(b), and 3(c). On the other hand, when the SMDOB-based SMC is used, even in the presence of sinusoidal functions in the references of the first and second joint positions (i.e., θ_{r1}, θ_{r2}), the joint positions θ_1 and θ_2 quickly converge to their references in approximately 2 s with a tracking error range of 0.2°. However, after 15 s, the step responses of the first and second joint positions

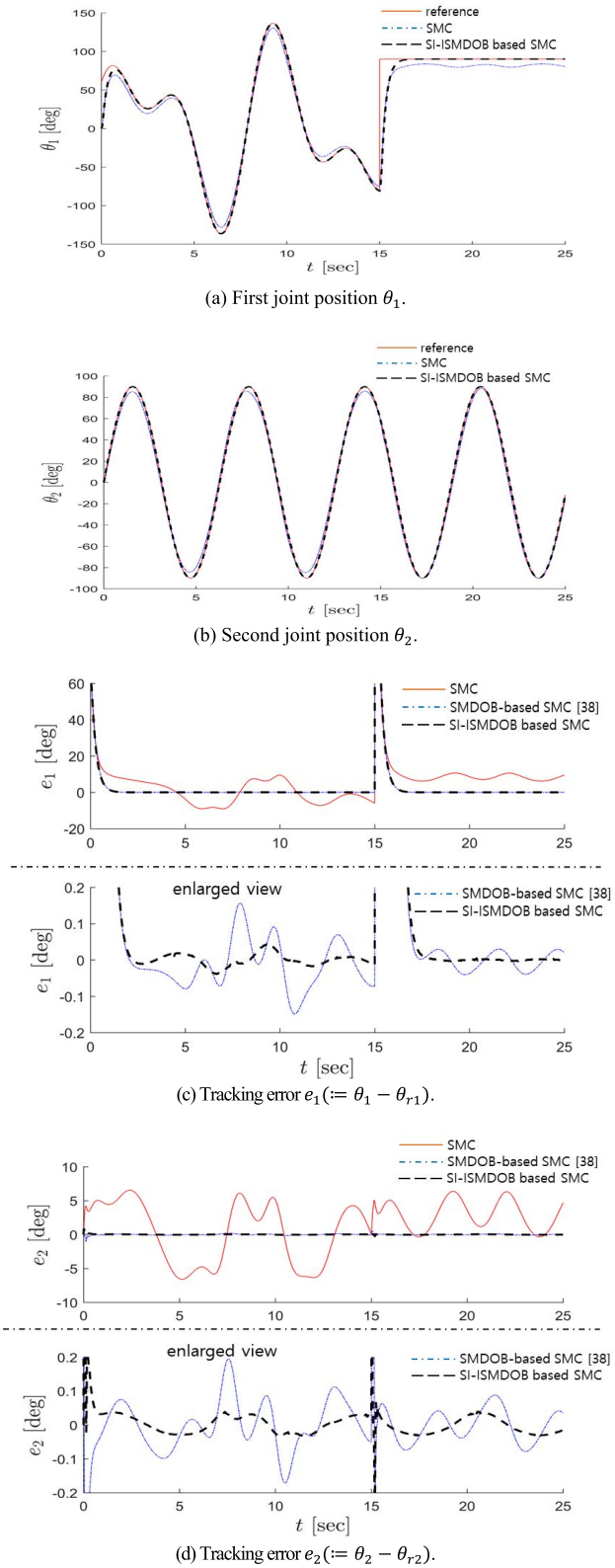

(a) First joint position θ_1.

(b) Second joint position θ_2.

(c) Tracking error $e_1 (:= \theta_1 - \theta_{r1})$.

(d) Tracking error $e_2 (:= \theta_2 - \theta_{r2})$.

FIGURE 3. Simulation results of the tracking performance using the proposed SI-ISMDOB-based SMC method.

still have tracking errors of 0.05° and 0.10°, respectively. On the other hand, when the SI-ISMDOB-based SMC is used, a tracking error of 0.05° is observed for the sinusoidal reference, and the tracking errors e_1 and e_2 converge to zero for the step response. Fig. 4 compares the first and second joint torque disturbances (τ_1, τ_2) and their estimates ($\hat{\tau}_1$, $\hat{\tau}_2$); the comparison proves that the estimation performance of the proposed ISMDOB for various types of disturbances is excellent.

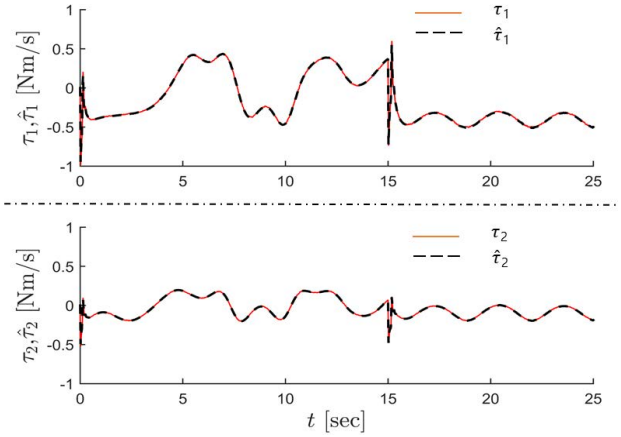

FIGURE 4. Simulation results of the estimate $\hat{\tau}_i$ of the torque disturbance τ_i using the proposed ISMDOB method.

B. EXPERIMENTAL ENVIRONMENTS

To verify the effectiveness of the proposed algorithm, an experimental environment was designed, as shown in Fig. 5. The control law is implemented using MATLAB/Simulink, and the control law constructed in the program using Quanser QUARC is interfaced with the experimental system. Using an NI PCIe-6351 data acquisition (DAQ) device, the sensor information from the actual system can be sent to MATLAB/Simulink, from which the control input can be transferred to the system.

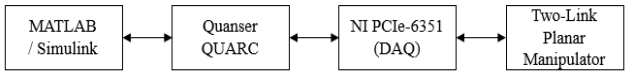

FIGURE 5. Interface environment between the proposed robust control system and the manipulator system.

The two-link manipulator model shown in Fig. 6 is equipped with DC motors (2324U006SR) and gear boxes (24/1 14:1), and gears with a 5:1 gear ratio are additionally attached to the manipulator to increase the torques of the DC motors to realize a final gear ratio of 70:1. The DC motors have encoders (IE2-512) that can measure the manipulator joint positions θ_1 and θ_2. Because the information from the encoders contains measurement noise and the experimental data is obtained from the actual two-link manipulator

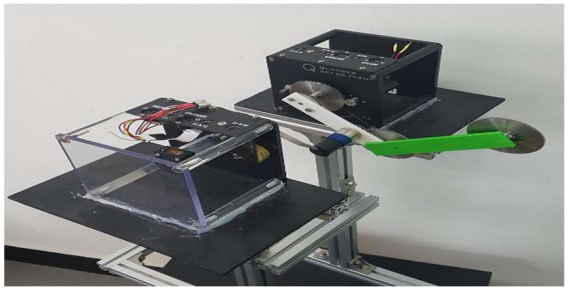

FIGURE 6. Actual manipulator system with an additional load.

system, the results obtained using this experimental setup demonstrate the validity of the proposed method in a noisy environment.

C. EXPERIMENTAL RESULTS

The parameters of the DC motor, manipulator, controller, and DOBs used in the experiments are the same as those listed in Tables 1–4. As in the simulations, the nonlinear characteristics of the robot manipulator dynamics are present in the experiments on the actual manipulator system. The identification error owing to the nonlinear characteristics of the manipulator-actuator dynamics, and the disturbances owing to the unknown load torque were compensated by the SI-ISMDOB-based SMC method. Experiments using the same reference values as in the simulations were conducted to confirm the validity of the proposed modeling method for the manipulator-actuator dynamics and disturbance compensation method. To this end, the performance of the proposed SI-ISMDOB-based SMC was compared to that of the SMC and SMDOB-based SMC [38] methods. In addition, to confirm the robust control performance, a mass object m_3 with a mass of 170.3 g was attached to the end of the second link to increase the uncertainties in the manipulator dynamics (i.e., torque disturbances). The experimental results without and with m_3 are shown in Figs. 7 and 8, respectively.

Fig. 7 shows the tracking errors using the i) SMC method, ii) SMDOB-based SMC method [38], and iii) SI-ISMDOB-based SMC method. When a DOB is not used in SMC, a relatively large error is generated, as shown in Figs. 7(a) and 7(b), similar to the one in the simulations. On the other hand, when DOBs are used, the reference is followed with a considerably small error range of 0.1°. In the case of the SMDOB-based SMC method, the error occurred in the second joint at approximately 18.6 s, as shown in Fig. 7(a). Although several experiments were performed to confirm that this phenomenon does not appear when using SI-ISMDOB-based SMC, the jagged motion appears in the case of the SI-ISMDOB method, as shown in Fig. 7(a). These phenomena were observed only in the experimental results, and not in the simulation results. In the experiments, uncertainties and disturbances can arise owing to numerous factors in the robot manipulator links and motor systems driving the links. Fig. 7(c) shows the

torque-disturbance estimates and the first and second joint voltage inputs (v_1, v_2) when using the SI-ISMDOB-based SMC.

Figs. 8(a) and 8(b) show the tracking errors when the object is attached to the end of the second link, and Fig. 8(c) shows the disturbance estimates and voltages when using the ISMDOB. When the DOB is not used, the maximum tracking error of the two joint positions becomes greater than 10°. In contrast, in the case of using the SI-ISMDOB-based SMC, the first joint shows a maximum error of 0.4° for a sinusoidal reference and 0.1° for the step reference; the second joint also shows an error of less than 0.2°. In the case of the SMDOB-based SMC, an error momentarily occurred in the first joint at approximately 5 s. Even if this phenomenon is neglected in the SMDOB-based SMC, both joints have relatively larger errors for a sinusoidal reference compared with that of the ISMDOB-based SMC. Based on the experimental results, the proposed SI-ISMDOB-based SMC method achieves the expected performance similar to that in simulations. Through a comparison of the proposed method, SMC, and SMDOB-based SMC, it is also validated that the proposed control method is effective in both simulations and experiments.

Tables 5-7 are provided for the analysis of the data present in Figs. 3, 4, 7 and 8. The normalizing performance indicator ρ, which was used in [45] and [46] for the performance evaluation of robot motion controllers, is used to evaluate the performance of SMC, SMDOB-based SMC, and SI-ISMDOB-based SMC methods for both simulation and experimental results. Table 5 (a) shows the simulation results of the first link of the manipulator. Both SMDOB-based SMC and ISMDOB-based SMC methods show the much less maximum error compared with those of SMC method. Although the maximum error velocity of the SMC method is somewhat smaller than SMDOB-based SMC and ISMDOB-based SMC methods, the performance indicators that considers both the maximum error velocity and maximum error show that ISMDOB-based SMC method achieve better performance than the other methods. In the case of second link as well, the improved performance of the ISMDOB-based SMC over SMC and SMDOB-based SMC can be more clearly seen in Table 5 (b). Tables 6 and 7 show the experimental results of maximum error velocity, maximum error, and performance indicator of the SMC, SMDOB-based SMC, and ISMDOB-based SMC methods. As shown in Table 6, the ISMDOB-based SMC shows much better performance in both the first and second links than SMC and SMDOB-based SMC. In the presence of additional load as well, the values of ISMDOB-based SMC remain much lower than those of SMC and SMDOB-based SMC in Tables 7. These results in Tables 5, 6, and 7 clearly demonstrate that the SI-ISMDOB-based SMC method results in the smallest value of ρ compared with both the SMC and SMDOB-based SMC methods, implying that the performance of the SI-ISMDOB-based SMC method is better than that of the SMC and SMDOB-based SMC methods in both the simulations and experiments.

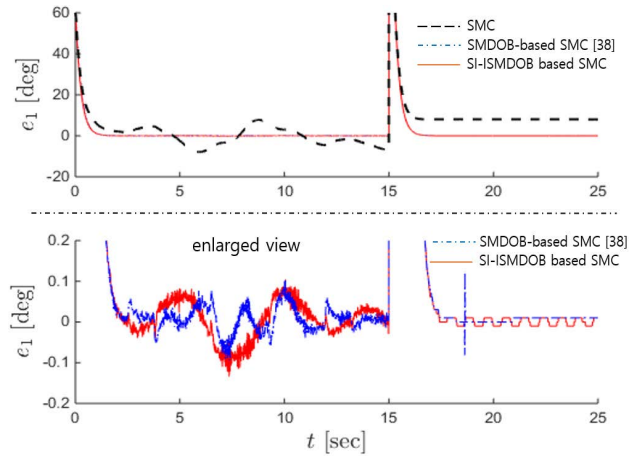

(a) Tracking error e_1.

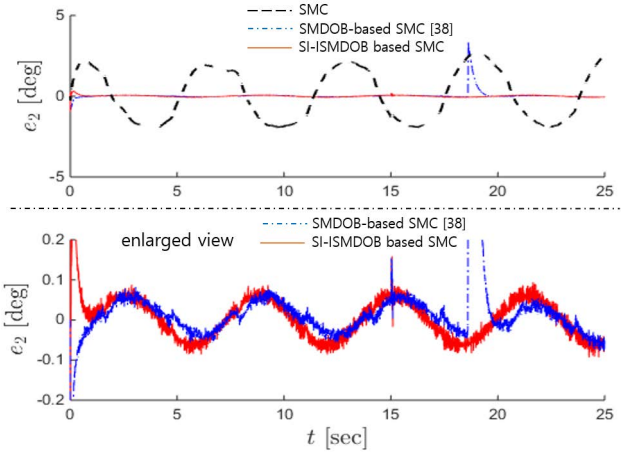

(b) Tracking error e_2.

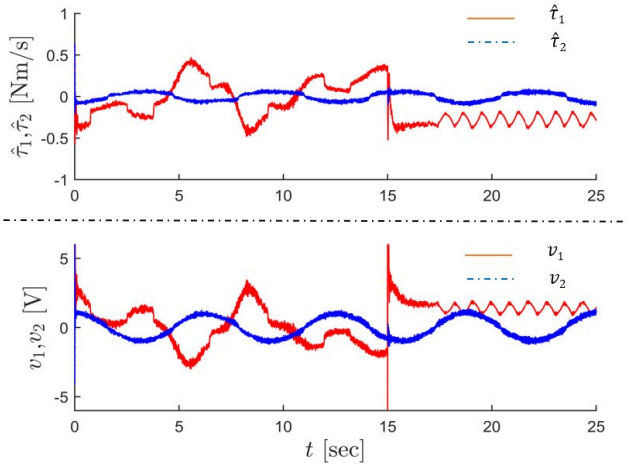

(c) Torque disturbance estimate $\hat{\tau}$ and torque input v using an ISMDOB.

FIGURE 7. Experimental results using the proposed SI-ISMDOB-based SMC method for the manipulator system without the additional load m_3.

It should be noted that the existing model-based control methods cannot be directly used for robot manipulators, unless their dynamics are available. In addition, most robust and adaptive model-free control strategies have been studied

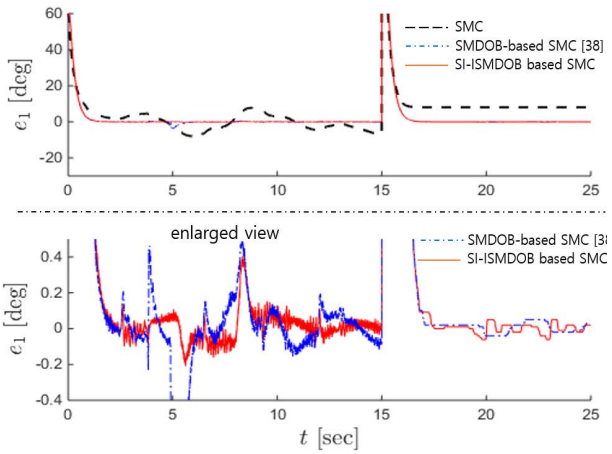

(a) Tracking error e_1.

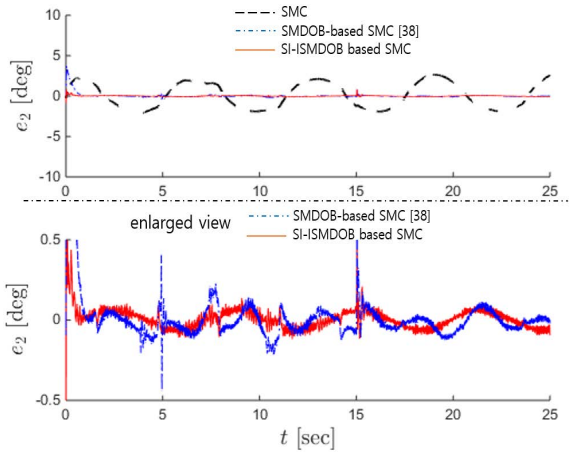

(b) Tracking error e_2.

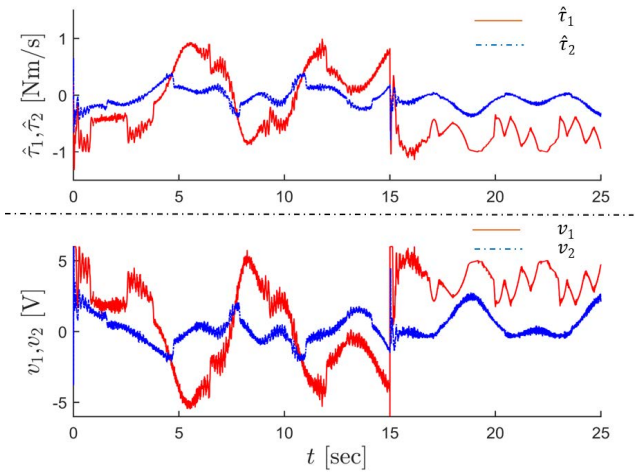

(c) Torque disturbance estimate $\hat{\tau}$ and torque input v using an ISMDOB.

FIGURE 8. Experimental results using the proposed SI-ISMDOB-based SMC method for the manipulator system with the additional load m_3.

TABLE 5. Simulation results of the performance indicator ρ of the SMC, SMDOB-based SMC, and SI-ISMDOB-based SMC methods.

(A) FIRST LINK

	Maximum error velocity $\lvert\dot{e}_1\rvert_{\max}$[rad/s]	Maximum error $\lvert e_1\rvert_{\max}$[rad]	ρ_1 (:= ratio of $\lvert e_1\rvert_{\max}$ to $\lvert\dot{e}_1\rvert_{\max}$) [s]
SMC	13.9520	9.6501	0.6917
SMDOB-based SMC	15.6905	1.5025	0.0958
SI-ISMDOB-based SMC	15.6847	1.4249	0.0908

(B) SECOND LINK

	Maximum error velocity $\lvert\dot{e}_2\rvert_{\max}$ [rad/s]	Maximum error $\lvert e_2\rvert_{\max}$[rad]	ρ_2 (:= ratio of $\lvert e_2\rvert_{\max}$ to $\lvert\dot{e}_2\rvert_{\max}$) [s]
SMC	96.8232	6.5961	0.0681
SMDOB-based SMC	90.0931	0.1951	0.0022
SI-ISMDOB-based SMC	90.0588	0.0387	0.0004

TABLE 6. Experimental results of the performance indicator ρ of the SMC, SMDOB-based SMC, and SI-ISMDOB-based SMC methods in the absence of additional load m_3.

(A) FIRST LINK

	Maximum error velocity $\lvert\dot{e}_1\rvert_{\max}$ [rad/s]	Maximum error $\lvert e_1\rvert_{\max}$[rad]	ρ_1 (:= ratio of $\lvert e_1\rvert_{\max}$ to $\lvert\dot{e}_1\rvert_{\max}$) [s]
SMC	19.7010	8.0357	0.4079
SMDOB-based SMC	21.6729	0.1221	0.0056
SI-ISMDOB-based SMC	22.3136	0.0102	0.0004

(B) SECOND LINK

	Maximum error velocity $\lvert\dot{e}_2\rvert_{\max}$[rad/s]	Maximum error $\lvert e_2\rvert_{\max}$[rad]	ρ_2 (:= ratio of $\lvert e_2\rvert_{\max}$ to $\lvert\dot{e}_2\rvert_{\max}$) [s]
SMC	21.7219	2.6557	0.1223
SMDOB-based SMC	24.6865	3.4054	0.1379
SI-ISMDOB-based SMC	22.3136	0.0976	0.0044

TABLE 7. Experimental results of the performance indicator ρ of the SMC, SMDOB-based SMC, and SI-ISMDOB-based SMC methods in the presence of additional load m_3.

(A) FIRST LINK

	Maximum error velocity $\lvert\dot{e}_1\rvert_{\max}$[rad/s]	Maximum error $\lvert e_1\rvert_{\max}$[rad]	ρ_1 (:= ratio of $\lvert e_1\rvert_{\max}$ to $\lvert\dot{e}_1\rvert_{\max}$) [s]
SMC	33.8942	7.9508	0.2346
SMDOB-based SMC	28.2385	4.4145	0.1536
SI-ISMDOB-based SMC	29.0017	0.4053	0.0140

(B) SECOND LINK

	Maximum error velocity $\lvert\dot{e}_2\rvert_{\max}$[rad/s]	Maximum error $\lvert e_2\rvert_{\max}$[rad]	ρ_2 (:= ratio of $\lvert e_2\rvert_{\max}$ to $\lvert\dot{e}_2\rvert_{\max}$) [s]
SMC	20.9511	2.1309	0.1017
SMDOB-based SMC	23.5932	0.4388	0.0186
SI-ISMDOB-based SMC	24.6592	0.1368	0.0055

for the systems other than the manipulator system. Therefore, it is difficult to compare the performance indicator ρ of the existing model-based methods or model-free methods and the proposed method for the considered unknown robot manipulator. Because several control objectives must be achieved, such as the nonlinear robust control of unknown robot manipulator system using system identification and

integral sliding mode disturbance observer methods, the overall proposed algorithm becomes complex. However, the algorithm of the proposed method was implemented in a robot manipulator system, and its feasibility was verified through experimental results.

V. CONCLUSION

The innovative features of this study are that manipulator-actuator dynamics are proposed and identified and then a nonlinear robust controller for an unknown actual robot manipulator system is designed, based on the identified manipulator-actuator dynamics and torque disturbance estimates. The identified manipulator-actuator dynamics with torque disturbances are obtained via system identification, and then the SI-ISMDOB-based SMC method is designed for the unknown robot manipulator system. In the simulations, the performance of the proposed method is verified for various reference joint positions. The validity of the proposed SI-ISMDOB-based method is also verified experimentally by implementing the proposed control strategy on a real manipulator system.

Because the unknown actuator dynamics, unknown manipulator parameters, frictional forces, and unknown load torques result in significant degradation of the manipulator control performance, the limitation of the existing methods (i.e., they cannot be employed for the unknown manipulator system) need to be overcome by developing the appropriate model, identification, and control methods for the unknown robot manipulator system. In contrast, the novelty of the proposed manipulator-actuator dynamics is clear in developing the robust manipulator control system since the manipulator dynamics consider all of the manipulator dynamics, actuator dynamics, unknown manipulator parameters, frictional forces, and the coupling between the motions of the manipulator links.

If an accurate model of the robot manipulator dynamics is available, then it is reasonable to use the model in the system control, as in the case of the existing model-based control methods. However, if this is not the case, then the proposed method can be significantly useful. In the proposed control method, there exists a tradeoff between the system model accuracy and the control performance of the robot manipulator system.

Finally, several issues regarding future possible studies are discussed. For nonlinear and robust adaptive control methods, the design parameters should be chosen through trial and error by observing the estimation and control performance. If the optimal design of the controller and observer parameters can be achieved by employing various optimization methods, such as particle swarm optimization, genetic algorithm, and artificial bee colony algorithm, the overall control performance of the manipulator system is expected to improve; this can be pursued in future studies. In addition, because the proposed method can be designed based only on the identified manipulator-actuator dynamics instead of the entire complex manipulator system dynamics, the proposed method can be extended to various practical systems and can handle control issues, such as image-based visual servoing of the manipulator system, which can be an interesting future work.

REFERENCES

[1] C. Tang, Y. Wang, S. Wang, R. Wang, and M. Tan, "Floating autonomous manipulation of the underwater biomimetic vehicle-manipulator system: Methodology and verification," *IEEE Trans. Ind. Electron.*, vol. 65, no. 6, pp. 4861–4870, Jun. 2018.

[2] J. Hu, H. Zhang, H. Liu, and X. Yu, "A survey on sliding mode control for networked control systems," *Int. J. Syst. Sci.*, vol. 52, no. 6, pp. 1129–1147, Apr. 2021.

[3] B. Wang, C. Zhang, Q. Jia, X. Liu, and G. Yang, "Robust continuous sliding mode control for manipulator PMSM trajectory tracking system under time-varying uncertain disturbances," *IEEE Access*, vol. 8, pp. 196618–196632, 2020.

[4] A. J. Munoz-Vazquez, J. D. Sanchez-Torres, E. Jimenez-Rodriguez, and A. G. Loukianov, "Predefined-time robust stabilization of robotic manipulators," *IEEE/ASME Trans. Mechatronics*, vol. 24, no. 3, pp. 1033–1040, Jun. 2019.

[5] B. Xiao, L. Cao, S. Xu, and L. Liu, "Robust tracking control of robot manipulators with actuator faults and joint velocity measurement uncertainty," *IEEE/ASME Trans. Mechatronics*, vol. 25, no. 3, pp. 1354–1365, Jun. 2020.

[6] A. T. Azar, F. E. Serrano, A. Koubaa, N. A. Mohamed, N. A. Kamal, I. K. Ibraheem, and A. J. Humaidi, "Sliding mode controller design for unmanned aerial vehicles with unmodeled polytopic dynamics," in *Unmanned Aerial Systems: Theoretical Foundation and Applications* (Advances in Nonlinear Dynamics and Chaos). New York, NY, USA: Academic, 2021, pp. 495–519.

[7] Z. Chen, F. Huang, W. Sun, J. Gu, and B. Yao, "RBF-neural-network-based adaptive robust control for nonlinear bilateral teleoperation manipulators with uncertainty and time delay," *IEEE/ASME Trans. Mechatronics*, vol. 25, no. 2, pp. 906–918, Apr. 2020.

[8] Z. Chen, F. Huang, W. Chen, J. Zhang, W. Sun, J. Chen, J. Gu, and S. Zhu, "RBFNN-based adaptive sliding mode control design for delayed nonlinear multilateral telerobotic system with cooperative manipulation," *IEEE Trans. Ind. Informat.*, vol. 16, no. 2, pp. 1236–1247, Feb. 2020.

[9] S. Mobayen, O. Mofid, S. U. Din, and A. Bartoszewicz, "Finite-time tracking controller design of perturbed robotic manipulator based on adaptive second-order sliding mode control method," *IEEE Access*, vol. 9, pp. 71159–71169, 2021.

[10] J. Baek, M. Jin, and S. Han, "A new adaptive sliding-mode control scheme for application to robot manipulators," *IEEE Trans. Ind. Electron.*, vol. 63, no. 6, pp. 3628–3637, Jun. 2016.

[11] T. N. Truong, A. T. Vo, and H.-J. Kang, "A backstepping global fast terminal sliding mode control for trajectory tracking control of industrial robotic manipulators," *IEEE Access*, vol. 9, pp. 31921–31931, 2021.

[12] W. Jie, Z. Yudong, B. Yulong, H. H. Kim, and M. C. Lee, "Trajectory tracking control using fractional-order terminal sliding mode control with sliding perturbation observer for a 7-DOF robot manipulator," *IEEE/ASME Trans. Mechatronics*, vol. 25, no. 4, pp. 1886–1893, Aug. 2020.

[13] S. M. Esmaeilzadeh, M. Golestani, and S. Mobayen, "Chattering-free fault-tolerant attitude control with fast fixed-time convergence for flexible spacecraft," *Int. J. Control, Autom. Syst.*, vol. 19, no. 2, pp. 767–776, Feb. 2021.

[14] B. Vaseghi, S. Mobayen, S. S. Hashemi, and A. Fekih, "Fast reaching finite time synchronization approach for chaotic systems with application in medical image encryption," *IEEE Access*, vol. 9, pp. 25911–25925, 2021.

[15] A. Q. Al-Dujaili, A. Falah, A. J. Humaidi, D. A. Pereira, and I. K. Ibraheem, "Optimal super-twisting sliding mode control design of robot manipulator: Design and comparison study," *Int. J. Adv. Robot. Syst.*, vol. 17, no. 6, pp. 1–17, Nov.-Dec. 2020.

[16] W.-H. Chen, D. J. Ballance, P. J. Gawthrop, and J. O'Reilly, "A nonlinear disturbance observer for robotic manipulators," *IEEE Trans. Ind. Electron.*, vol. 47, no. 4, pp. 932–938, Aug. 2000.

[17] A. Mohammadi, M. Tavakoli, H. J. Marquez, and F. Hashemzadeh, "Nonlinear disturbance observer design for robotic manipulators," *Control Eng. Pract.*, vol. 21, no. 3, pp. 253–267, Mar. 2013.

[18] S. Komada, N. Machii, and T. Hori, "Control of redundant manipulators considering order of disturbance observer," *IEEE Trans. Ind. Electron.*, vol. 47, no. 2, pp. 413–420, Apr. 2000.
[19] W. R. Abdul-Adheem, I. K. Ibraheem, A. J. Humaidi, and A. T. Azar, "Model-free active input–output feedback linearization of a single-link flexible joint manipulator: An improved active disturbance rejection control approach," *Meas. Control*, vol. 54, nos. 5–6, pp. 856–871, Jun. 2020.
[20] W. He, A. O. David, Z. Yin, and C. Sun, "Neural network control of a robotic manipulator with input deadzone and output constraint," *IEEE Trans. Syst., Man, Cybern., Syst.*, vol. 46, no. 6, pp. 759–770, Jun. 2016.
[21] G. A. R. Ibraheem, A. T. Azar, I. K. Ibraheem, and A. J. Humaidi, "A novel design of a neural network-based fractional PID controller for mobile robots using hybridized fruit fly and particle swarm optimization," *Complexity*, vol. 2020, pp. 1–18, Apr. 2020.
[22] R. Rahmani, S. Mobayen, A. Fekih, and J.-S. Ro, "Robust passivity cascade technique-based control using RBFN approximators for the stabilization of a cart inverted pendulum," *Mathematics*, vol. 9, no. 11, p. 1229, May 2021.
[23] Q. Zhou, H. Li, and P. Shi, "Decentralized adaptive fuzzy tracking control for robot finger dynamics," *IEEE Trans. Fuzzy Syst.*, vol. 23, no. 3, pp. 501–510, Jun. 2015.
[24] Z. Chen, F. Huang, C. Yang, and B. Yao, "Adaptive fuzzy backstepping control for stable nonlinear bilateral teleoperation manipulators with enhanced transparency performance," *IEEE Trans. Ind. Electron.*, vol. 67, no. 1, pp. 746–756, Jan. 2020.
[25] C. Mingyue and W. Zhaojing, "Stochastic modeling and control of manipulator with elastic joint actuated by DC-motors," in *Proc. 36th Chin. Control Conf. (CCC)*, Dalian, China, Jul. 2017, pp. 1949–1954.
[26] R. J. Wai and P. C. Chen, "Robust neural-fuzzy-network control for robot manipulator including actuator dynamics," *IEEE Trans. Ind. Electron.*, vol. 53, no. 4, pp. 1328–1349, Jun. 2006.
[27] L. Cheng, Z.-G. Hou, and M. Tan, "Adaptive neural network tracking control for manipulators with uncertain kinematics, dynamics and actuator model," *Automatica*, vol. 45, no. 10, pp. 2312–2318, 2009.
[28] F. H. Ajeil, I. K. Ibraheem, A. J. Humaidi, and Z. H. Khan, "A novel path planning algorithm for mobile robot in dynamic environments using modified bat swarm optimization," *J. Eng.*, vol. 2021, no. 1, pp. 37–48, Feb. 2021.
[29] L. Wang, T. Chai, and L. Zhai, "Neural-network-based terminal sliding mode control of robotic manipulators including actuator dynamics," *IEEE Trans. Ind. Electron.*, vol. 56, no. 9, pp. 3296–3304, Sep. 2009.
[30] T. Sun, H. Pei, Y. Pan, H. Zhou, and C. Zhang, "Neural network-based sliding mode adaptive control for robot manipulators," *Neurocomputing*, vol. 74, nos. 14–15, pp. 2377–2384, Jul. 2011.
[31] R. J. Wai and R. Muthusamy, "Fuzzy-neural-network inherited sliding mode control for robot manipulator including actuator dynamics," *IEEE Trans. Neural Netw. Learn. Syst.*, vol. 24, no. 2, pp. 274–287, Feb. 2013.
[32] W. He, H. Gao, C. Zhou, C. Yang, and Z. Li, "Reinforcement learning control of a flexible two-link manipulator: An experimental investigation," *IEEE Trans. Syst., Man, Cybern. Syst.*, vol. 51, no. 12, pp. 7326–7336, Dec. 2021.
[33] Z.-J. Yang, Y. Fukushima, and P. Qin, "Decentralized adaptive robust control of robot manipulators using disturbance observers," *IEEE Trans. Control Syst. Technol.*, vol. 20, no. 5, pp. 1357–1365, Sep. 2012.
[34] S.-H. Hsu and L.-C. Fu, "Adaptive decentralized control of robot manipulators driven by current-fed induction motors," *IEEE/ASME Trans. Mechatron.*, vol. 10, no. 4, pp. 465–468, Aug. 2005.
[35] L. Ljung, *System Identification: Theory for the User*. Upper Saddle River, NJ, USA: Prentice-Hall, 1999.
[36] M. T. Hamayun, C. Edwards, and H. Alwi, *Fault tolerant control schemes using integral sliding modes, Studies in Systems*, vol. 61. Mexico. Cancun: Decision and Control Book 2020.
[37] V. Utkin, J. Guldner, and J. Shi, *Sliding Mode Control in Electromechanical System*. London U.K.: Taylor & Francis, 1999.
[38] D. Chwa, "Robust nonlinear disturbance observer based adaptive guidance law against uncertainties in missile dynamics and target maneuver," *IEEE Trans. Aerosp. Electron. Syst.*, vol. 54, no. 4, pp. 1739–1749, Aug. 2018.
[39] H. K. Khalil, *Nonlinear Systems*. Upper Saddle River, NJ, USA: Prentice-Hall, 2002.
[40] J. Li, *Global Finite Time Stabilization by Output Feedback for Nonlinear Systems*. Morrisville, NC, USA: ProQuest, 2007.
[41] H. J. Palanthandalam-Madapusi, A. J. Ridley, and D. S. Bernstein, "Identification and prediction of ionospheric dynamics using a Hammerstein-Wiener model with radial basis functions," in *Proc. Amer. Control Conf.*, Portland, OR, USA, Jun. 2005, pp. 5052–5057.
[42] J. Várès, "An iterative method for Wiener-Hammerstein systems parameter identification," *J. Electr. Eng.*, vol. 58, no. 2, pp. 114–117, Jan. 2007.
[43] B. Ding and B. Huang, "Output feedback model predictive control for nonlinear systems represented by Hammerstein-Wiener model," *IET Control Theory Appl.*, vol. 1, no. 5, pp. 1302–1310, Sep. 2007.
[44] B. Xian, M. S. de Queiroz, D. M. Dawson, and M. L. McIntyre, "A discontinuous output feedback controller and velocity observer for nonlinear mechanical systems," *Automatica*, vol. 40, no. 3, pp. 695–700, Apr. 2004.
[45] W.-H. Zhu, T. Lamarche, E. Dupuis, D. Jameux, P. Barnard, and G. Liu, "Precision control of modular robot manipulators: The VDC approach with embedded FPGA," *IEEE Trans. Robot.*, vol. 29, no. 5, pp. 1162–1179, Oct. 2013.
[46] J. Mattila, J. Koivumaki, D. G. Caldwell, and C. Semini, "A survey on control of hydraulic robotic manipulators with projection to future trends," *IEEE/ASME Trans. Mechatronics*, vol. 22, no. 2, pp. 669–680, Apr. 2017.

DONGKYOUNG CHWA received the B.S. and M.S. degrees in control and instrumentation engineering and the Ph.D. degree in electrical and computer engineering from Seoul National University, Seoul, South Korea, in 1995, 1997, and 2001, respectively.

From 2001 to 2003, he was a Postdoctoral Researcher with Seoul National University, where he was also a BK21 Assistant Professor, in 2004. Since 2005, he has been with the Department of Electrical and Computer Engineering, Ajou University, Suwon-si, South Korea, where he is currently a Professor. He was a Visiting Scholar with the Australian Defence Force Academy, University of New South Wales Canberra; The University of Melbourne, Melbourne, VIC, Australia, in 2003; and the University of Florida, Gainesville, in 2011. His research interests include nonlinear, robust, and adaptive control theories and their applications to robotics; underactuated systems, including wheeled mobile robots; underactuated ships; cranes; and guidance and control of flight systems.

HEEJUN KWON received the B.S. degree in mechanical engineering and the M.S. degree in electrical and computer engineering from Ajou University, Suwon-si, South Korea, in 2017 and 2019, respectively.

Since 2019, he has been with FASTECH, Bucheon-si, South Korea, where he is currently an Associate Researcher. His research interests include nonlinear, robust, and adaptive control theories and their applications to motor systems, robotics, and underactuated systems.